Tunable structural phase transition and superconductivity in the Weyl semimetal Mo_{1−x}W_{x}Te_{2}

R. Dahal, L. Z. Deng, N. Poudel, M. Gooch, Z. Wu, H. C. Wu, H. D. Yang, C. K. Chang, and C. W. Chu

Phys. Rev. B **101**, 140505 — Published 16 April 2020

DOI: 10.1103/PhysRevB.101.140505

Tunable Structural Phase Transition and Superconductivity in Weyl Semimetal $Mo_{1-x}W_xTe_2$

R. Dahal[1], L. Z. Deng[1], N. Poudel[2], M. Gooch[1], Z. Wu[1], H. C. Wu[1,3], H. D. Yang[3,4], C. K. Chang[5], and C. W. Chu[1,6]

[1] *Texas Center for Superconductivity and Department of Physics, University of Houston, Houston, TX 77204, USA*

[2] *Idaho National Laboratory, Idaho Falls, ID 83402, USA*

[3] *Department of Physics, National Sun Yat-sen University, Kaohsiung, 80424, Taiwan*

[4] *Center of Crystal Research, National Sun Yat-sen University, Kaohsiung, 80424, Taiwan*

[5] *National Synchrotron Radiation Research Center, Hsinchu, 30076, Taiwan and*

[6] *Lawrence Berkeley National Laboratory, 1 Cyclotron Road, Berkeley, CA 94720, USA*

(Dated: March 24, 2020)

The relationship among structural transition, superconductivity, and doping in the Weyl semimetal $Mo_{1-x}W_xTe_2$ has been established through a systematic study of the doping and pressure effects. Doping-dependent resistivity measurements at ambient pressure revealed that the structural transition temperature increases linearly with increasing W content in $Mo_{1-x}W_xTe_2$. The observed structural transition temperature (T_s) of $MoTe_2$ at ambient pressure is 249 K and that of WTe_2 is 613 K. Temperature-dependent synchrotron X-ray diffraction measurements further confirmed the structural transition in WTe_2 at ambient pressure. Pressure was found to continuously suppress the T_s in $Mo_{0.90}W_{0.10}Te_2$, $Mo_{0.60}W_{0.40}Te_2$, and $Mo_{0.25}W_{0.75}Te_2$, and superconductivity emerges in $Mo_{0.90}W_{0.10}Te_2$ and $Mo_{0.60}W_{0.40}Te_2$ above 1.25 K when T_s is suppressed to a lower temperature.

Transition-metal dichalcogenides (TMDs) have been extensively investigated due to their wide-ranging electronic, optical, chemical, thermal, and mechanical properties, which are useful for device applications [1–7]. TMDs have a common formula MX_2, where M refers to a transition metal of group IVB (Ti, Zr, or Hf), VB (V, Nb, or Ta), or VIB (Cr, Mo, or W), and X is a chalcogen (S, Se, or Te) [8, 9]. Most of the TMDs crystallize into a 2-D layered structure [10, 11], in which each monolayer consists of transition-metal atoms between two planes of chalcogens (X-M-X). Atoms within a layer have a strong covalent bond, while interlayer bonding between the adjacent planes is by weak van der Waals-type forces. This feature gives rise to crystals that can be cleaved easily, and many of their physical properties are anisotropic [12]. TMDs can display semiconducting, semimetallic, or metallic behavior, which correlates well with the crystalline phase [13].

$MoTe_2$ and WTe_2 are both Weyl semimetals [14–17] with extremely large non-saturating magnetoresistance (MR) and interesting physical properties [18, 19]. The observed non-saturating MR for $MoTe_2$ at 2 K and an applied field of 33 T is 61,700%, while that for WTe_2 is even more impressive, 13,000,000% at 0.53 K and an applied field of 60 T. When WTe_2 is thinned to a single monolayer, it becomes a 2D topological insulator with a conducting edge, in which a superconducting transition can be driven by applying a gate voltage [20, 21]. Additionally, a dome-shaped superconducting behavior has been observed in both $MoTe_2$ and WTe_2 under pressure, with a maximum superconducting transition temperature (T_c) of 8.2 K at 11.7 GPa in $MoTe_2$ [22] and 7 K at 16.8 GPa in WTe_2 [23]. The Weyl semimetal state has also been observed in $Mo_{1-x}W_xTe_2$ for $x = 0.75$ and this compound has been predicted to be a tunable Weyl semimetal by varying x [24].

Depending on the synthesis conditions, $Mo_{1-x}W_xTe_2$ can crystalize into one of three different phases: the hexagonal 2H phase (space group $P6_3/mmc$), the monoclinic 1T′ phase (space group $P2_1/m$), or the orthorhombic T_d phase (space group $Pmn2_1$) [10, 25–28]. The 2H phase is semiconducting, whereas the 1T′ and T_d phases are semimetallic. For $x \leq 0.10$, the compound is semiconducting at ambient conditions, while it is semimetallic above 900 C, which can be stabilized at room temperature by rapid cooling. The compound is semimetallic for $x > 0.10$, independent of synthesis conditions. Rapid cooling of $MoTe_2$ results in the compound being in the 1T′ phase at room temperature, whereas that of WTe_2 results in T_d phase. Thus, depending on the doping level in $Mo_{1-x}W_xTe_2$, the semimetallic phase can exhibit either 1T′ or T_d structure at room temperature [27].

The semimetallic 1T′-phase $MoTe_2$ undergoes a structural transition at $\sim$ 250 K to the T_d phase at ambient [29, 30]. External pressure suppresses the structural transition temperature (T_s) in $MoTe_2$ and, by suppressing the T_s to lower temperatures, the superconducting transition temperature (T_c) can be increased from 0.10 K at ambient to 8.2 K at 11.7 GPa [22, 31, 32]. No structural transition in WTe_2 at ambient pressure has been reported to date. Kang *et al.* found no structural transition up to 20.1 GPa in WTe_2 by conducting synchrotron X-ray diffraction (XRD) at room temperature [33], while Zhuo *et al.* and Lu *et al.* both observed a room-temperature structural transition in WTe_2 starting under 6 GPa and 4 GPa, respectively, by conducting synchrotron XRD [34, 35]. Pressure is a basic and clean tuning parameter since it can have a great effect on physical and structural properties [31, 36] by reducing atomic distances and shifting a compound's Fermi levels without complications arising from changing the chemistry of the compound. To explore the phase diagram of,

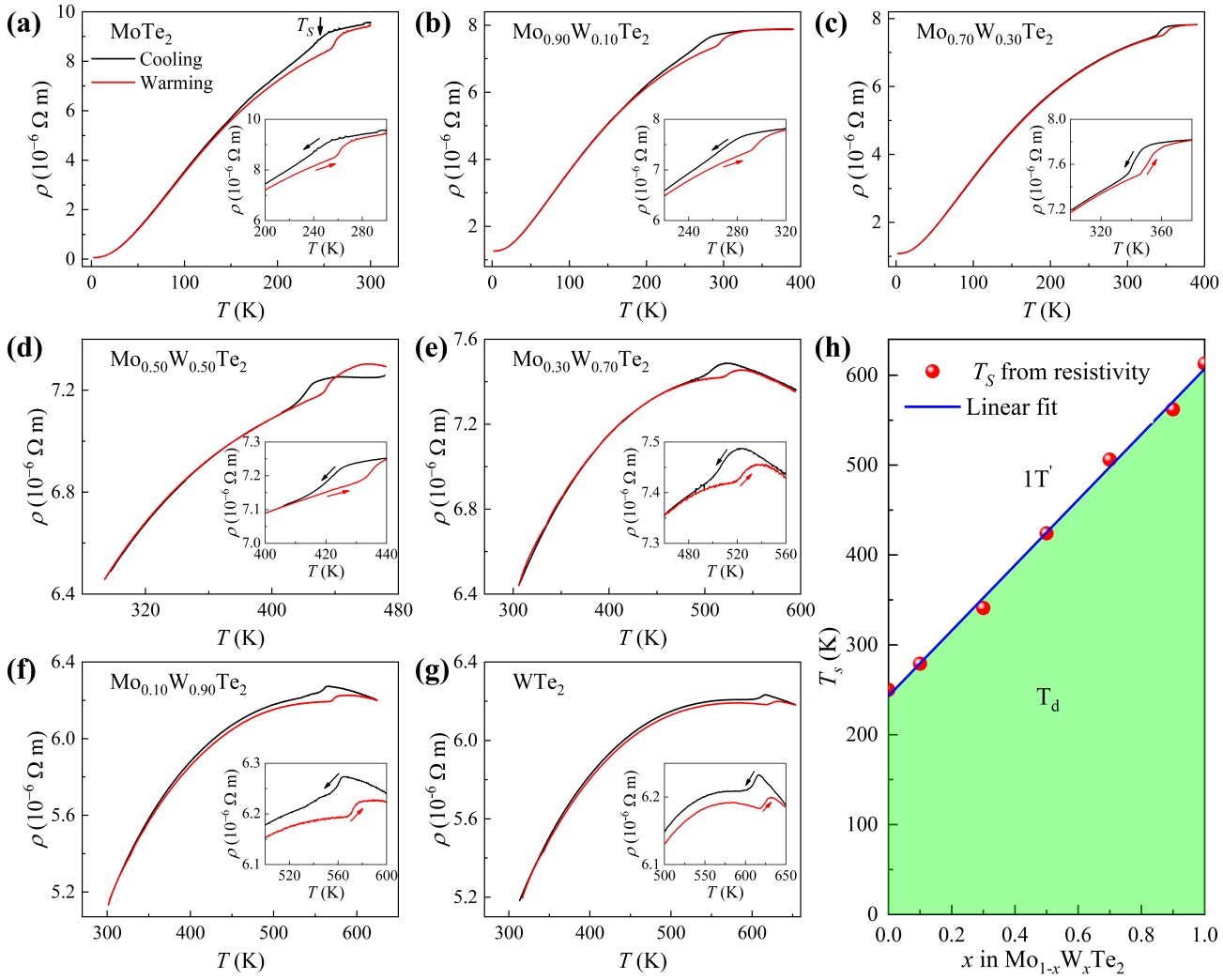

FIG. 1. Temperature-dependent resistivity of $Mo_{1-x}W_xTe_2$ in different temperature regions from 2 K to 650 K for x = (a) 0; (b) 0.10; (c) 0.30 (d) 0.50; (e) 0.70; (f) 0.90 and (g) 1, respectively. Insets to (a) - (g) show anomalies with thermal hysteresis associated with the structural transition from the monoclinic 1T′ phase to the orthorhombic T_d phase. In (a) - (g), black curves correspond to the cooling cycles and red curves correspond to the warming cycles. (h) Variation of structural transition temperature T_s with doping in $Mo_{1-x}W_xTe_2$ obtained from resistivity measurements. T_s is taken at the maxima of $d\rho/dT$ during the cooling cycles.

and the effects of external pressure on, $Mo_{1-x}W_xTe_2$, we have conducted resistivity measurements on single crystals with selected doping levels under different pressures. The results show the relationship between T_s and W-doping x at ambient pressure and the suppression of T_s with increasing pressure, accompanied by the emergence of superconductivity.

Single crystals of $MoTe_2$ and WTe_2 were grown by the flux method described elsewhere [37, 38]. Doped single crystals of $Mo_{1-x}W_xTe_2$ with nominal composition x = 0.10, 0.30, 0.40, 0.50, 0.70, 0.75, and 0.90 were prepared by the chemical vapor transport method using iodine as the transport agent following Ref. [27]. Synthesis details can be found in the Supplemental Material [39]. The compositions determined by energy-dispersive X-ray spectroscopy (EDS) are shown in Table S1 in the Supplemental Material.

To investigate the relation between T_s and W-concentration x, resistivity measurements up to 650 K were conducted for x = 0, 0.10, 0.30, 0.50, 0.70, 0.90, and 1, as shown in Figures 1(a)-(g). A clear hysteresis was observed in the resistivity for $MoTe_2$, which is associated with the first-order structural transition from the monoclinic 1T′ phase to the orthorhombic T_d phase at T_s = 249 K, consistent with previous reports [11, 22, 29]. This anomaly was also observed for all other samples with different doping. The T_ss for the doped samples are 279 K, 341 K, 424 K, 506 K, 562 K, and 613 K for

$x = 0.10, 0.30, 0.50, 0.70, 0.90$, and 1, respectively. T_s increases linearly with increasing x, as shown in Fig. 1(h). It has been reported that the 1T′ phase has a slightly smaller equilibrium volume than the T_d phase in $MoTe_2$ [22]. Since W has a slightly larger atomic radius than Mo, an increase in x enlarges the equilibrium volume, the T_d phase with a larger equilibrium volume becomes energetically favorable, and more active energy is required to convert the T_d phase into the 1T′ phase as mentioned in Ref. [28], leading to a higher T_s, which could explain the observed increase in T_s with increasing W concentration across the phase diagram.

In order to verify the structural transition and to obtain further structural information above T_s, WTe_2, which has the highest T_s, was selected for temperature-dependent synchrotron XRD measurements in the temperature range from 300 K to 673 K. At 300 K, the orthorhombic T_d phase with the non-centrosymmetric space group $Pmn2_1$ is detected, as shown in Fig. 2(a), consistent with a previous report [26], and it persists up to 573 K. As the temperature increases to 598 K, a new Bragg reflection peak emerges, suggesting the breaking of the crystal symmetry. The new Bragg reflection peak was indexed as a 013 peak (Fig. 2(b)) with the monoclinic centrosymmetric 1T′ phase ($P2_1/m$). As the temperature further increases, the intensity of the 013 peak increases as well, indicating the development of the 1T′ phase. At 673 K the structure is completely transformed to the 1T′ phase. Thus, the temperature-dependent synchrotron XRD results for WTe_2 are consistent with our resistivity measurement data.

To study the pressure effects on the doped compounds, single crystals with $x = 0.10, 0.40$, and 0.75 were investigated. At ambient pressure, $Mo_{0.90}W_{0.10}Te_2$ exhibits a ρ anomaly at T_s associated with the structural transition, as shown in Fig. 3(a).The ρ anomaly at T_s, characteristic of the 1T′-to-T_d transition, diminishes with pressure up to 13.52 kbar and is no longer observable at 17.71 kbar (see Fig. S1 in the Supplemental Material for hysteresis effects). A slight drop in ρ was observed at 3.89 kbar at 1.26 K. This ρ drop becomes more pronounced with increasing pressure and reaches zero at 13.52 kbar, which indicates the emergence of superconductivity at a transition temperature $T_c \sim 2.7$ K. With increasing pressure, the T_c continues to increase, and a T_c of 3.6 K is reached at 17.71 kbar.

No structural transition was detected for $Mo_{0.60}W_{0.40}Te_2$ at ambient pressure from room temperature down to 1.25 K, as shown in Fig. 3(b). However, a structural transition was observed at 244 K under 3.28 kbar, and T_s continuously decreases to $\sim$ 65 K as pressure increases up to 16.66 kbar (see Fig. S2 in the Supplemental Material for hysteresis effects). Superconductivity was observed at 1.59 K around 8.35 kbar and T_c continuously increases to 2.6 K with further increasing pressure.

Initially, no ρ anomaly was observed in $Mo_{0.25}W_{0.75}Te_2$ at ambient pressure from room

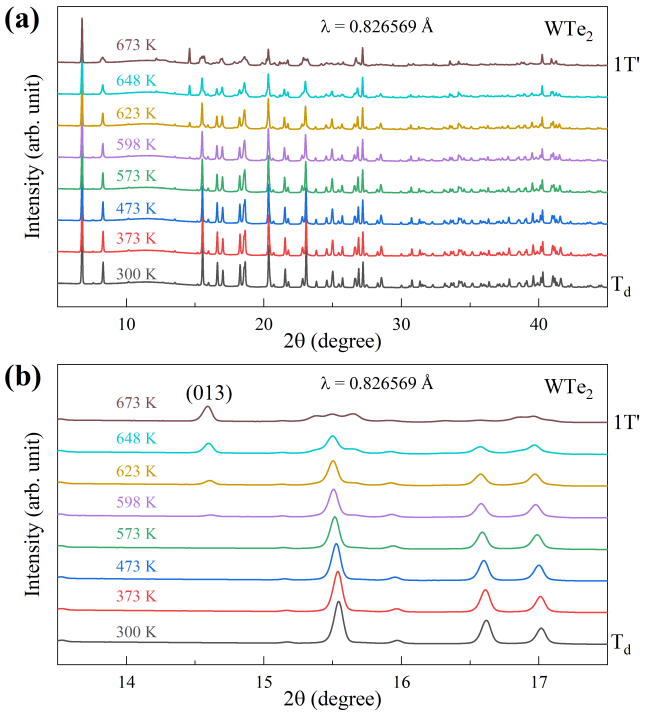

FIG. 2. Temperature-dependent synchrotron X-ray diffraction (XRD) patterns for WTe_2 (a) from 5 to 45 degrees and (b) from 13.5 to 17.5 degrees.

temperature down to 1.25 K, as shown in Fig. 3(c). However, as the pressure increases, the overall resistivity decreases, and at $\sim$ 12.32 kbar a ρ anomaly with hysteresis (see Fig. S3 in the Supplemental Material), which is associated with a first-order structural transition [29], appears at 245 K. With further increasing pressure, the T_s is suppressed to around 180 K at 17.05 kbar, but superconductivity was not observed down to 1.25 K.

Temperature - pressure (T - P) phase diagrams for $x = 0.10$, $x = 0.40$, and $x = 0.75$ are shown in Figures 3(d-f), respectively. In all three compounds, increasing pressure continuously suppresses the T_s. We also found that pressures higher than 3.28 kbar are needed to suppress the T_s to below room temperature for $x \geq 0.40$. It has been reported that a structural transition in WTe_2 is observed at room temperature under pressures of 4 to 6 GPa [34, 35]. In addition, pressure has also been found to suppress the T_s of $MoTe_2$ [31, 32]. These observations support the existence of a structural transition in $Mo_{1-x}W_xTe_2$ at ambient pressure for all x, with higher T_s at higher W concentration. Among these three compounds, superconductivity was observed for $x = 0.10$ and $x = 0.40$. The T_c increases with pressure and the dT_c/dP is 0.17 K/kbar for $x = 0.10$ and 0.11 K/kbar for $x = 0.40$.

Competition between the structural transition and superconductivity in $Mo_{1-x}W_xTe_2$ is supported by the following observations. With increasing pressure, T_s continuously decreases, as shown in Figures 3(d - f). Once the

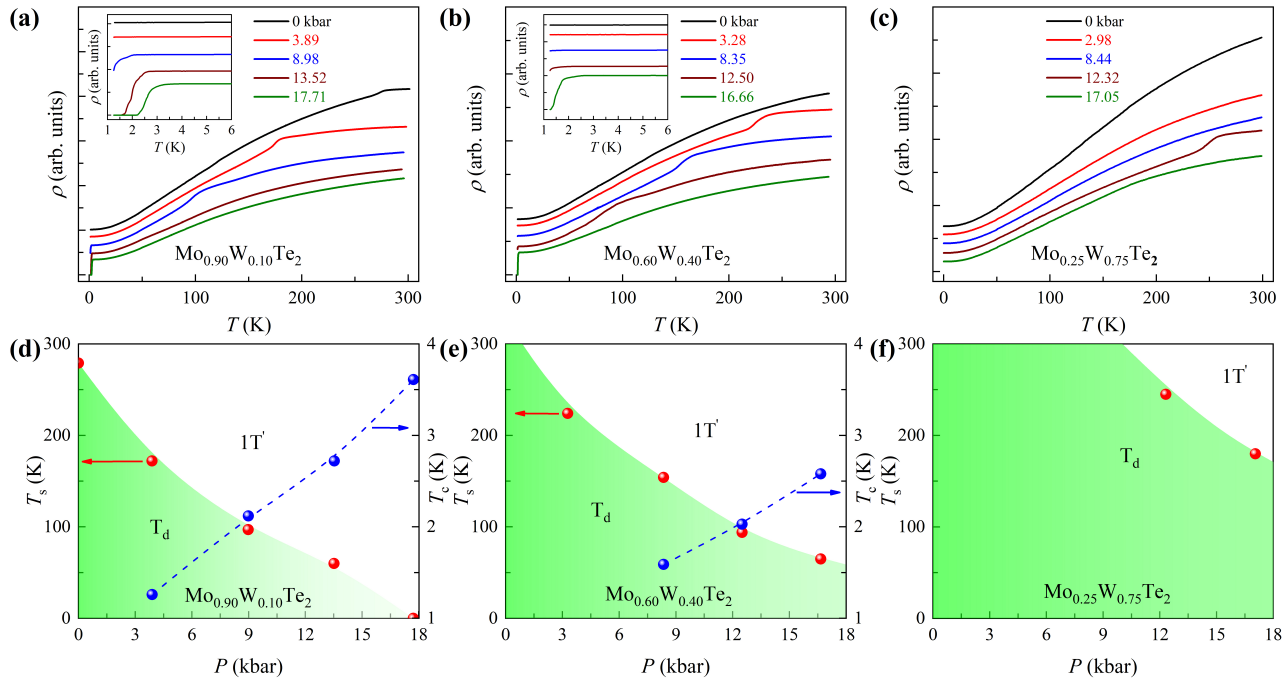

FIG. 3. Temperature-dependent resistivity of (a) $Mo_{0.90}W_{0.10}Te_2$, (b) $Mo_{0.60}W_{0.40}Te_2$, and (c) $Mo_{0.25}W_{0.75}Te_2$ at various pressures. For clarity, the resistivity curves have been shifted vertically. The anomaly in the resistivity corresponds to the structural transition from the monoclinic 1T′ phase to the orthorhombic T_d phase. Insets to (a) and (b) show low-temperature-region data for $Mo_{0.90}W_{0.10}Te_2$ and $Mo_{0.60}W_{0.40}Te_2$, respectively. (d) and (e) Pressure-dependent structural transition (red spheres) and superconductivity (blue spheres) for $Mo_{0.90}W_{0.10}Te_2$ and $Mo_{0.60}W_{0.40}Te_2$, respectively. (f) Pressure-dependent structural transition for $Mo_{0.25}W_{0.75}Te_2$.

T_s is suppressed to < 175 K, superconductivity emerges (e.g. for $x = 0.10$ with a $T_c = 1.26$ K under 3.89 kbar and for $x = 0.40$ with a $T_c = 1.59$ K under 8.35 kbar). An increase in the T_c is coupled with the decrease of the T_s. Superconductivity was not observed for $x = 0.75$ down to 1.25 K with T_s down to $\sim$ 180 K and under pressures up to 17 kbar. It has been previously reported that pressure continuously suppresses T_s in $MoTe_2$ [22, 32, 40] and that a sharp increase in T_c is observed in the pressure range from 2.7 to 7.5 kbar [31]. There have also been reports of pressure-induced structural transition in WTe_2 at room temperature [34, 35]. However, our observation shows that WTe_2 has a structural transition at ambient pressure with $T_s = 613$ K; therefore, the previously reported structural transition under pressure in WTe_2 is more likely be related to the suppression of the structural transition rather than being induced under pressure. Clarke *et al.* reported that although the structural transition in $MoTe_2$ at ambient pressure occurs around 250 K, two phases coexist in an extended temperature range from 233 K to 290 K [30]. Heikes *et al.* have also shown that the 1T′ and T_d phases co-exist in $MoTe_2$ at 1.5 K and under hydrostatic pressure of 1 GPa [32]. Once the T_s in $Mo_{1-x}W_xTe_2$ is suppressed by pressure to below critical temperature, completion of the structural transition occurs at very low temperature, after which the T_c sharply increases. These observations shed light on the possible origin(s) for the superconductivity in $Mo_{1-x}W_xTe_2$ system, such as the competition between the superconductivity and the structural transition, and/or the co-existence of different phases.

Total energy calculations including the van der Waals interaction have shown that the T_d phase is energetically more stable than the 1T′ phase [41]. The energy differences between the T_d and 1T′ phases in $MoTe_2$ and WTe_2 are 0.40 and 0.46 meV per unit cell, respectively. This suggests that higher energy is required for the transition from the T_d phase to the 1T′ phase in WTe_2 than in $MoTe_2$. It has been reported that the interlayer contraction increases the hybridization between the Te p_z orbitals, resulting in the enhancement of the three-dimensionality of the band character [42]. Since the atomic radius of W is larger than that of Mo, an increase in W content expands the interlayer distance in $Mo_{1-x}W_xTe_2$ and reduces interlayer hybridization. Total kinetic energy of the electron increases as interlayer hybridization decreases [31]. The increase in kinetic energy leads to an increase in the total energy, assuming the rest changes negligibly. Thus, the energy difference between the T_d phase and the 1T′ phase increases with increasing W composition. When the energy difference is larger, higher energy (and hence higher temperature) is required for the transition from the T_d phase to the 1T′ phase, which explains the increasing T_s with increasing

W content as shown in Fig. 1(h). On the other hand, the application of external pressure reduces the interlayer distance and enhances the interlayer hybridization, which leads to a lower T_s and favors superconductivity.

Applying pressure to $MoTe_2$/WTe_2 suppresses the interlayer Te-Te distances while the intralayer Mo-Te/W-Te [22, 35] bond length is almost unchanged due to the anisotropy of the van der Waals structure. P. Lu et al. [35] pointed out that one transverse acoustic vibrational mode, mainly from Te-Te interlayer vibrations, contributes significantly to the electron-phonon coupling. It is thus natural to suggest that the pressure effect on $Mo_{1-x}W_xTe_2$ also leads to the softening of the interlayer Te-Te vibration modes. The superconducting transition temperature T_c can be estimated by the modified McMillan formula [43]:

$$T_c = \frac{\langle\omega\rangle}{1.20}\exp\Big(-\frac{1.04(1+\lambda)}{\lambda-\mu^*(1+0.62\lambda)}\Big), \qquad (1)$$

where the parameter $\langle\omega\rangle$ is the average of phonon energy defined as $\langle\omega\rangle = \frac{2}{\lambda}\int_0^\infty d\omega\ \alpha^2F(\omega)$, μ^* is the Coulomb pseudopotential, and λ is the dimensionless electron-phonon coupling strength. λ in terms of the Eliashberg electron-phonon spectral function $\alpha^2F(\omega)$ is expressed as $\lambda = 2\int_0^\infty d\omega\ \alpha^2F(\omega)/\omega$, where α^2 is an average of the electron-phonon interaction, $F(\omega)$ is the phonon density of states, and ω is the phonon frequency. The phonon softening can result in an increase in the superconducting transition temperature, which could possibly be the origin of the emergence of superconductivity in $Mo_{1-x}W_xTe_2$ under high pressure.

In conclusion, the structural phase diagram of $Mo_{1-x}W_xTe_2$ at ambient pressure has been established. Resistivity measurements at ambient pressure and at temperatures up to 650 K have revealed some previously unreported structural phase transitions. T_s linearly increases with increasing W content from $MoTe_2$ to WTe_2, which is due to enhancement in the kinetic energy of the system with W doping. Additionally, the T - P phase diagrams of $Mo_{1-x}W_xTe_2$ for $x = 0.25$, $x = 0.40$, and $x = 0.75$ have been constructed. Based on our high-pressure resistivity measurements, we conclude that there is a competition between the structural transition and superconductivity in $Mo_{1-x}W_xTe_2$, in which superconductivity emerges when T_s is suppressed to < 175 K and, as T_s is further suppressed, T_c increases.

The work in Houston is supported in part by U.S. Air Force Office of Scientific Research Grant No. FA9550-15-1-0236, the T. L. L. Temple Foundation, the John J. and Rebecca Moores Endowment, and the State of Texas through the Texas Center for Superconductivity at the University of Houston.

[1] J. A. Wilson and A. D. Yoffe, Adv. Phys. **18**, 193 (1969).
[2] Q. H. Wang, K. Kalantar-Zadeh, A. Kis, J. N. Coleman, and M. S. Strano, Nat. Nanotechnol. **7**, 699 (2012).
[3] A. D. Yoffe, Annu. Rev. Mater. Sci. **3**, 147 (1973).
[4] R. C. Morris, R. V. Coleman, and R. Bhandari, Phys. Rev. B **5**, 895 (1972).
[5] B. Sipos, A. F. Kusmartseva, A. Akrap, H. Berger, L. Forró, and E. Tutiš, Nat. mater. **7**, 960 (2008).
[6] B. W. H. Baugher, H. O. H. Churchill, Y. Yang, and P. Jarillo-Herrero, Nat. nanotechnol. **9**, 262 (2014).
[7] X. Qian, J. Liu, L. Fu, and J. Li, Science **346**, 1344 (2014).
[8] H. Katzke, P. Tolédano, and W. Depmeier, Phys. Rev. B **69**, 134111 (2004).
[9] A. R. Beal and H. P. Hughes, J. Phys. C: Solid State Phys. **12**, 881 (1979).
[10] B. E. Brown, Acta Crystallogr. **20**, 268 (1966).
[11] T. Zandt, H. Dwelk, C. Janowitz, and R. Manzki, J. Alloys and Compounds **442**, 216 (2007).
[12] J. E. Callanan, G. Hope, R. D. Weir, and E. F. Westrum, J. Chem. Thermodynamics **24**, 627 (1992).
[13] F. Zhang, H. Zhang, S. Krylyuk, C. A. Milligan, Y. Zhu, D. Y. Zemlyanov, L. A. Bendersky, B. P. Burton, A. V. Davydov, and J. Appenzeller, Nat. Mater. **18**, 55 (2019).
[14] M. Sakano, M. S. Bahramy, H. Tsuji, I. Araya, K. Ikeura, H. Sakai, S. Ishiwata, K. Yaji, K. Kuroda, A. Harasawa, S. Shin, and K. Ishizaka, Phys. Rev. B **95**, 121101 (2017).
[15] J. Jiang, Z. K. Liu, Y. Sun, H. F. Yang, C. R. Rajamathi, Y. P. Qi, L. X. Yang, C. Chen, H. Peng, C. C. Hwang, S. Z. Sun, S.-K. Mo, I. Vobornik, J. Fujii, S. S. P. Parkin, C. Felser, B. H. Yan, and Y. L. Chen, Nat. Commun. **8**, 13973 (2017).
[16] Y.-Y. Lv, X. Li, B.-B. Zhang, W. Y. Deng, S.-H. Yao, Y. B. Chen, J. Zhou, S.-T. Zhang, M.-H. Lu, L. Zhang, M. Tian, L. Sheng, and Y.-F. Chen, Phys. Rev. Lett. **118**, 096603 (2017).
[17] P. Li, Y. Wen, X. He, Q. Zhang, C. Xia, Z.-M. Yu, S. A. Yang, Z. Zhu, H. N. Alshareef, and X.-X. Zhang, Nat. Commun. **8**, 2150 (2017).
[18] X. Luo, F. C. Chen, J. L. Zhang, Q. L. Pei, G. T. Lin, W. J. Lu, Y. Y. Han, C. Y. Xi, W. H. Song, and Y. P. Sun, Appl. Phys. Lett. **109**, 102601 (2016).
[19] M. N. Ali, J. Xiong, S. Flynn, J. Tao, Q. D. Gibson, L. M. Schoop, T. Liang, N. Haldolaarachchige, M. Hirschberger, N. P. Ong, and R. J. Cava, Nature (London) **514**, 205 (2014).
[20] Z. Fei, T. Palomaki, S. Wu, W. Zhao, X. Cai, B. Sun, P. Nguyen, J. Finney, X. Xu, and D. H. Cobden, Nat. Phys. **13**, 677 (2017).
[21] E. Sajadi, T. Palomaki, Z. Fei, W. Zhao, P. Bement, C. Olsen, S. Luescher, X. Xu, J. A. Folk, and D. H. Cobden, Science **362**, 922 (2018).
[22] Y. Qi, P. G. Naumov, M. N. Ali, C. R. Rajamathi, W. Schnelle, O. Barkalov, M. Hanfland, S.-C. Wu, C. Shekhar, Y. Sun, V. Süß, M. Schmidt, U. Schwarz, E. Pippel, P. Werner, R. Hillebrand, T. Förster, E. Kampert, S. Parkin, R. J. Cava, C. Felser, B. Yan, and S. A. Medvedev, Nat. Commun. **7**, 11038 (2016).
[23] X.-C. Pan, X. Chen, H. Liu, Y. Feng, Z. Wei, Y. Zhou, Z. Chi, L. Pi, F. Yen, F. Song, X. Wan, Z. Yang, B. Wang,

G. Wang, and Y. Zhang, Nat. Commun. **6**, 7805 (2015).
[24] I. Belopolski, D. S. Sanchez, Y. Ishida, X. Pan, P. Yu, S.-Y. Xu, G. Chang, T.-R. Chang, H. Zheng, N. Alidoust, G. Bian, M. Neupane, S.-M. Huang, C.-C. Lee, Y. Song, H. Bu, G. Wang, S. Li, G. Eda, H.-T. Jeng, T. Kondo, H. Lin, Z. Liu, F. Song, S. Shin, and M. Z. Hasan, Nat. Commun. **7**, 13643 (2016).
[25] Y.-Y. Lv, L. Cao, X. Li, B.-B. Zhang, K. Wang, B. Pang, L. Ma, D. Lin, S.-H. Yao, J. Zhou, Y. B. Chen, S.-T. Dong, W. Liu, M.-H. Lu, Y. Chen, and Y.-F. Chen, Sci. Rep. **7**, 44587 (2017).
[26] W. G. Dawson and D. W. Bullett, J. Phys. C: Solid State Phys. **20**, 6159 (1987).
[27] S. M. Oliver, R. Beams, S. Krylyuk, I. Kalish, A. K. Singh, A. Bruma, F. Tavazza, J. Joshi, I. R. Stone, S. J. Stranick, A. V. Davydov, and P. M. Vora, 2D Mater. **4**, 045008 (2017).
[28] X.-J. Yan, Y.-Y. Lv, L. Li, X. Li, S.-H. Yao, Y.-B. Chen, X.-P. Liu, H. Lu, M.-H. Lu, and Y.-F. Chen, Appl. Phys. Lett. **110**, 211904 (2017).
[29] H. P. Hughes and R. H. Friend, J. Phys. C: Solid State Phys. **11**, L103 (1978).
[30] R. Clarke, E. Marseglia, and H. P. Hughes, Philos. Mag. B **38**, 121 (1978).
[31] H. Takahashi, T. Akiba, K. Imura, T. Shiino, K. Deguchi, N. K. Sato, H. Sakai, M. S. Bahramy, and S. Ishiwata, Phys. Rev. B **95**, 100501(R) (2017).
[32] C. Heikes, I.-L. Liu, T. Metz, C. Eckberg, P. Neves, Y. Wu, L. Hung, P. Piccoli, H. Cao, J. Leao, J. Paglione, T. Yildirim, N. P. Butch, and W. Ratcliff, Phys. Rev. Mater. **2**, 074202 (2018).
[33] D. Kang, Y. Zhou, W. Yi, C. Yang, J. Guo, Y. Shi, S. Zhang, Z. Wang, C. Zhang, S. Jiang, A. Li, K. Yang, Q. Wu, G. Zhang, L. Sun, and Z. Zhao, Nat. Commun. **6**, 7804 (2015).
[34] Y. Zhou, X. Chen, N. Li, R. Zhang, X. Wang, C. An, Y. Zhou, X. Pan, F. Song, B. Wang, W. Yang, Z. Yang, and Y. Zhang, AIP Adv. **6**, 075008 (2016).
[35] P. Lu, J.-S. Kim, J. Yang, H. Gao, J. Wu, D. Shao, B. Li, D. Zhou, J. Sun, D. Akinwande, D. Xing, and J.-F. Lin, Phys. Rev. B **94**, 224512 (2016).
[36] L. Z. Deng, Y. P. Zheng, Z. Wu, S. Huyan, H.-C. Wu, Y. F. Nie, K. Cho, and C.-W. Chu, Proc. Natl. Acad. Sci. USA **116**, 2004 (2019).
[37] J. Yang, J. Colen, J. Liu, M. C. Nguyen, G.-w. Chern, and D. Louca, Sci. Adv. **3**, eaao4949 (2017).
[38] E. J. Sie, C. M. Nyby, C. D. Pemmaraju, S. J. Park, X. Shen, J. Yang, M. C. Hoffmann, B. K. Ofori-Okai, R. Li, A. H. Reid, S. Weathersby, E. Mannebach, N. Finney, D. Rhodes, D. Chenet, A. Antony, L. Balicas, J. Hone, T. P. Devereaux, T. F. Heinz, X. Wang, and A. M. Lindenberg, Nature (London) **565**, 61 (2019).
[39] See Supplemental Material for experimental methods.
[40] Y. J. Hu, Y. T. Chan, K. T. Lai, K. O. Ho, X. Guo, H.-P. Sun, K. Y. Yip, D. H. L. Ng, H.-Z. Lu, and S. K. Goh, Phys. Rev. Mater. **3**, 034201 (2019).
[41] H.-J. Kim, S.-H. Kang, I. Hamada, and Y.-W. Son, Phys. Rev. B **95**, 180101(R) (2017).
[42] K. Ikeura, H. Sakai, M. S. Bahramy, and S. Ishiwata, APL Mater. **3**, 041514 (2015).
[43] R. C. Dynes, Solid State Commun. **10**, 615 (1972).